Journal of Advanced Ceramics
2017, **6**(2): 110–119
DOI: 10.1007/s40145-017-0223-7

ISSN 2226-4108
CN 10-1154/TQ

Research Article

Preparation and characterization of high-performance ZrB_2–SiC–C_f composites sintered at 1450 ℃

Wenhu HONG[a,†], Kaixuan GUI[b,†], Ping HU[b,c,*], Xinghong ZHANG[b], Shun DONG[b]

[a]*China Academy of Launch Vehicle Technology*, *Beijing 100000*, *China*
[b]*National Key Laboratory of Science and Technology on Advanced Composites in Special Environments*, *Harbin Institute of Technology*, *Harbin 150001*, *China*
[c]*Key Laboratory of Materials Physics*, *Institute of Solid State Physics*, *Chinese Academy of Sciences*, *Hefei 230031*, *China*

Received: December 15, 2016; Revised: March 08, 2017; Accepted: March 17, 2017

Abstract: ZrB_2–SiC–C_f composites containing 20–50 vol% short carbon fibers were hot pressed at low sintering temperature (1450 ℃) using nanosized ZrB_2 powders, in which the fiber degradation was effectively inhibited. The strain-to-failure values of such composites increased with increasing fiber content, and the value for the composite with 50 vol% C_f was even more than 3 times higher than that of the composite with 20 vol% C_f. Furthermore, the composite exhibited non-brittle fracture mode when the fiber content was above 30 vol%, and the thermal shock critical temperature difference of the composite with 30 vol% C_f was up to 727 ℃, revealing excellent thermal shock resistance of this composite. Additionally, ZrB_2–SiC–C_f composites displayed good oxidation resistance when the fiber content was below 40 vol%, suggesting that this method provides a promising way for preparation of high-performance ZrB_2–SiC–C_f composites at low temperature.

Keywords: ceramics; fibers; microstructure; thermal shock resistance; oxidation resistance

1 Introduction

In recent years, ultra-high temperature ceramics (UHTCs) have attracted much attention because of their unique combination of properties, including high melting point, great strength, high electrical and thermal conductivities, excellent corrosion resistance, as well as good oxidation resistance [1]. ZrB_2 has a relatively low density compared with other UHTCs, which makes it a promising material for use in extreme environments, such as sharp leading edge and control surface components on hypersonic vehicles [2–4]. ZrB_2–SiC composites are currently considered as the baseline ultra-high temperature ceramic composites owing to the fact that the introduction of SiC not only improves the mechanical properties of ZrB_2 by inhibiting the grain growth during sintering, but also increases the oxidation resistance of ZrB_2 by promoting the formation of silicate-based glasses that inhibit oxidation at temperatures between 800 and 1700 ℃ [5]. However, the inherent brittleness and poor thermal shock resistance of ZrB_2–SiC ceramics are still obstacles for their engineering applications [6]. Therefore, great efforts have been employed to toughen ZrB_2-based composites and push forward their application limits, and a variety of reinforcements such as particles [7],

† Wenhu Hong and Kaixuan Gui contributed equally to this work.
* Corresponding author.
E-mail: huping123hit@163.com

graphite flakes [8], whiskers [9], and fibers [10,11] have been adopted to toughen ZrB_2-based UHTCs through different toughening mechanisms. Among these, fiber with large aspect ratio is the most promising reinforcement due to its effective toughening mechanisms (e.g., fiber pullout, fiber–matrix interface debonding, crack deflection, and fiber bridging). Meanwhile, carbon additives, for example in the form of carbon black [12,13], fiber [14–17], nanotube [18,19], graphite [8,20], or graphene [21,22], can react with and eliminate the surface oxide impurities, which promote the sinterability by minimizing the grain growth in ZrB_2–SiC composites.

Carbon fiber has demonstrated its feasibility as structural material in aerospace and aeronautic industries due to its high strength, low density, and good thermal stability. It is also a very good reinforcement in strengthening and/or toughening ceramics and improving thermal shock resistance of ceramics [23]. Recently, researchers have become increasingly concerned about the carbon fiber reinforced ZrB_2-based ceramics since they offer a great potential for improving the fracture toughness and thermal shock resistance of ZrB_2-based UHTCs. Nevertheless, one of the obstacles for real application of the composites is the degradation of carbon fibers caused by fiber graphitization as well as the reaction between ceramic matrix and fibers at high sintering temperature [24].

Researchers have shown that severe degradation of carbon fibers is detected in ZrB_2- or HfB_2-based ceramics by hot pressing at high temperatures (2000–2100 ℃) and just a few fibers are pulled out from the fracture surfaces of materials [25–28]. Similar results were obtained in the carbon fiber reinforced ZrB_2-based composites fabricated by SPS at 1900 ℃ with a short sintering time [16], indicating that the high sintering temperature rather than sintering time is the dominant factor that causes the degradation of carbon fibers. Thereby, it is necessary to reduce the sintering temperature of carbon fiber reinforced ZrB_2-based ceramic composites. The strategy typically adopted to lower the sintering temperature and enhance sinterability of ZrB_2 is to use nanosized powders as starting material instead of micron sized powders since the sintering activity of nanosized particles is dramatically higher than that of their micron sized counterparts [29–32]. No open literature has reported the fabrication of ZrB_2–SiC–C_f composites by low temperature (below 1500 ℃) hot pressing using nanosized ZrB_2 powders, and the thermal shock resistance of these composites has not been reported as well to the best of our knowledge.

In the present work, we attempt to fabricate carbon fiber reinforced ZrB_2–SiC composites by hot pressing at low temperature using nanosized ZrB_2 powders to avoid fiber degradation. In addition, the influences of carbon fiber volume fraction on the relative density, microstructure, mechanical properties, oxidation resistance, as well as thermal shock resistance of the composites were systematically investigated.

2 Experimental process

Commercially available ZrB_2 powders (D_{50} = 150 nm, > 99% purity, Beijing HWRK Chem Co. Ltd., China), SiC powders (D_{50} = 0.45 μm, > 99% purity, Kaihua, China), and T800 carbon fibers (5 μm in diameter, Torayca Co. Ltd., Tokyo, Japan) were used as raw materials. The carbon fibers were chopped into ~2 mm short fibers. The ZrB_2 and 20 vol% SiC powders containing 20–50 vol% carbon fibers were ultrasonically dispersed (KR-1200, KER Co. Ltd., Shenyang, China) for 1 h and then ball milled (GCQM-2L, GCKY Co. Ltd., Nanjing, China) for 10 h in a polyethylene bottle using WC balls and ethanol as the grinding media. To minimize segregation caused by sedimentation during drying, the slurry was dried in a rotary evaporator (R502B, Shensheng Technology Co. Ltd., Shanghai, China) at 75 ℃ in a vacuum of 200 mm Hg with a rotation speed of 40 rpm. Figure 1 shows the scanning electron microscopy (SEM) images of the starting ZrB_2 powders and the mixed ZrB_2–20 vol% SiC–30 vol% C_f powders. The dried powders were heated in a resistance-heated graphite furnace (CXZT-45-23Y, Chen Xin Electric Furnace Co. Ltd., Shanghai, China) at 15 ℃/min in vacuum (~20 Pa) to 1450 ℃ with a uniaxial load of 30 MPa and a dwelling time of 2 h at this temperature. After sintering, the furnace was cooled at ~20 ℃/min to room temperature. Table 1 shows the name and composition of samples prepared in the present study.

Table 1 Name and composition of samples produced in the present study

Sample name	ZrB_2 (vol%)	SiC (vol%)	C_f (vol%)
ZSC20	60	20	20
ZSC30	50	20	30
ZSC40	40	20	40
ZSC50	30	20	50

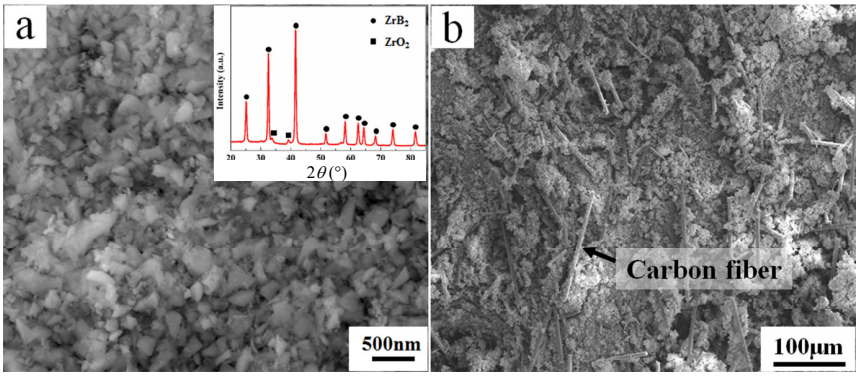

Fig. 1 SEM images of (a) the starting ZrB_2 powders (inset is the X-ray diffraction pattern) and (b) the mixed ZrB_2–20 vol% SiC–30 vol% C_f powders, showing the powders with an average particle size of 150 nm and the uniform distribution of carbon fibers in the ceramic powders.

The bulk densities of sintered specimens were measured by the Archimedes' method with deionized water as the immersing medium. Relative densities were calculated dividing bulk densities by the theoretical densities based on the law of mixture.

Flexural strength was tested in three-point bending on 3 mm × 4 mm × 36 mm bars, using a 30 mm span and a crosshead speed of 0.5 mm/min. Fracture toughness was evaluated by a single-edge notched beam (SENB) method with a 16 mm span using 2 mm × 4 mm × 22 mm test bars and a crosshead speed of 0.05 mm/min. Specimens for flexural strength and fracture toughness testing were prepared by diamond polishing to a 0.5 μm finish, and the reported averages and standard deviations were calculated from a minimum of six bars.

A water-quenching technique was used for thermal shock tests. The specimens were heated at a rate of 10 ℃/min to a preset temperature (200–800 ℃) in a resistance furnace in air and held at this temperature for 30 min. Then, the specimens were subjected to thermal shock by quenching them into water bath from the preset temperatures, and the residual flexural strengths of the specimens after quenching were measured by three-point bending test. The measured thermal shock critical temperature difference (ΔT_c) value was defined as 70% of the room temperature strength, which was determined using linear interpolation of the residual strength values as described in ASTM C1525-04 [33].

The oxidation behavior of the samples was investigated using isothermal tests at 1500 ℃ in static air for 1 h.

Microstructure of the samples was analyzed by scanning electron microscopy (SEM, FEI Sirion, Holland) with energy dispersion spectroscopy (EDS), transmission electron microscopy, and high-resolution transmission electron microscopy (TEM and HR-TEM, Tecnai G^2-F30, USA). The preparation of TEM samples was performed by focused ion beam (FIB, FEI 600i, USA).

3 Results and discussion

3.1 Microstructure

SEM images of the polished surfaces of ZrB_2–SiC–C_f composites are shown in Fig. 2. Short fibers with an average length of ~150 μm are uniformly distributed among ceramic matrix, lower than their original length (~2 mm). The decrease in fiber length is caused by both the colliding of WC balls during ball milling and the applied pressure during sintering [34].

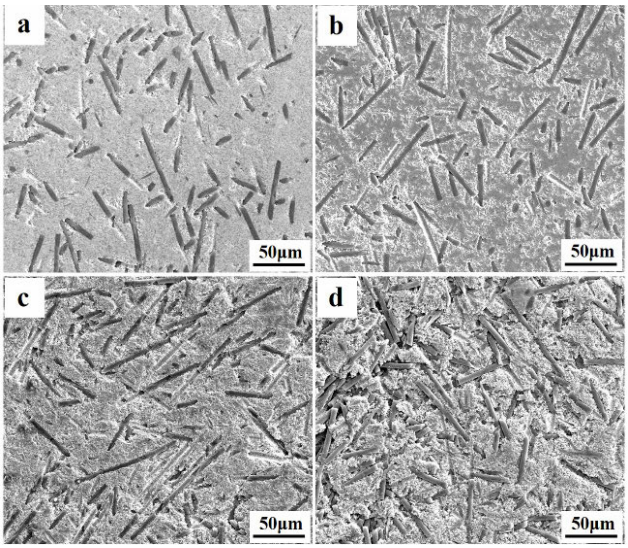

Fig. 2 SEM images of the polished surfaces of ZrB_2–SiC–C_f composites: (a) ZSC20, (b) ZSC30, (c) ZSC40, and (d) ZSC50, showing a uniform distribution of carbon fibers in the composites.

Figure 3 shows the microstructures of fracture surfaces of ZrB_2–SiC–C_f composites, in which the structural integrity of the fibers is well preserved implying that the degradation of fibers is effectively inhibited owing to the low sintering temperature. In addition, fiber debonding and pullout are clearly observed on the fracture surfaces of ZrB_2–SiC–C_f composites and the average pullout length increases with the increasing fiber content. The interfacial bonding strength between fibers and ceramic matrix can be evaluated by the fiber pullout length. An extensive fiber pullout indicates a relatively weak fiber–matrix interfacial bonding, while a flat fracture surface suggests a strong fiber–matrix interfacial bonding [35]. This interaction between the fibers and matrix determines the fracture mode of the composite, that is, a strong interface leads to a brittle composite, whereas a weak interface allows fiber debonding and the composite exhibits a non-brittle failure mode [36]. ZSC20 exhibits a strong fiber–matrix interfacial bonding since few fibers pull out from the fracture surface resulting in a brittle fracture mode of this sample, whereas numerous fibers pull out from the fracture surface of ZSC30 leading to a non-brittle fracture mode and an increased fracture toughness of this sample compared with that of ZSC20. However, further increase in fiber content has a negative effect on the improvement of fracture toughness of the composite, which could be ascribed to the significant reduction of relative density.

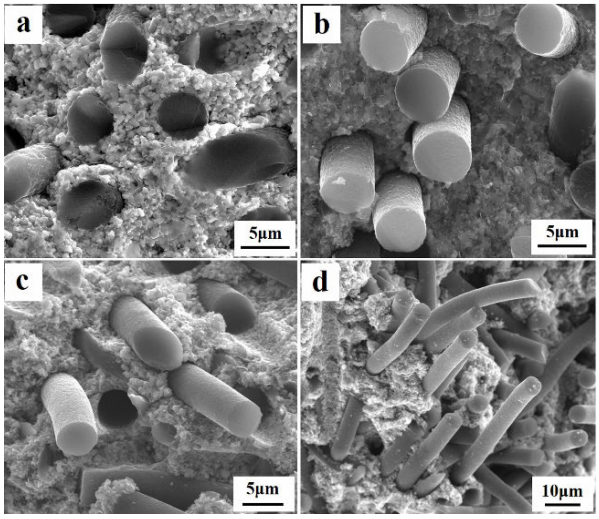

Fig. 3 SEM images of the fracture surfaces of ZrB_2–SiC–C_f composites: (a) ZSC20, (b) ZSC30, (c) ZSC40, and (d) ZSC50, showing that the structural integrity of carbon fibers is well preserved and that the average fiber pullout length increases with increasing fiber content.

TEM analysis was also performed for ZSC30 to further characterize the interfaces between fibers and ceramic matrix. The bright field image and element distribution on the observed area of ZSC30 are exhibited in Fig. 4. In addition to the main elements, including Zr, B, Si, and C, a certain amount of O element is also detected. According to the element distribution in ZSC30, the corresponding phases including ZrB_2, SiC, ZrO_2, and carbon fiber are marked in Fig. 4, in which ZrO_2 impurity mainly comes from

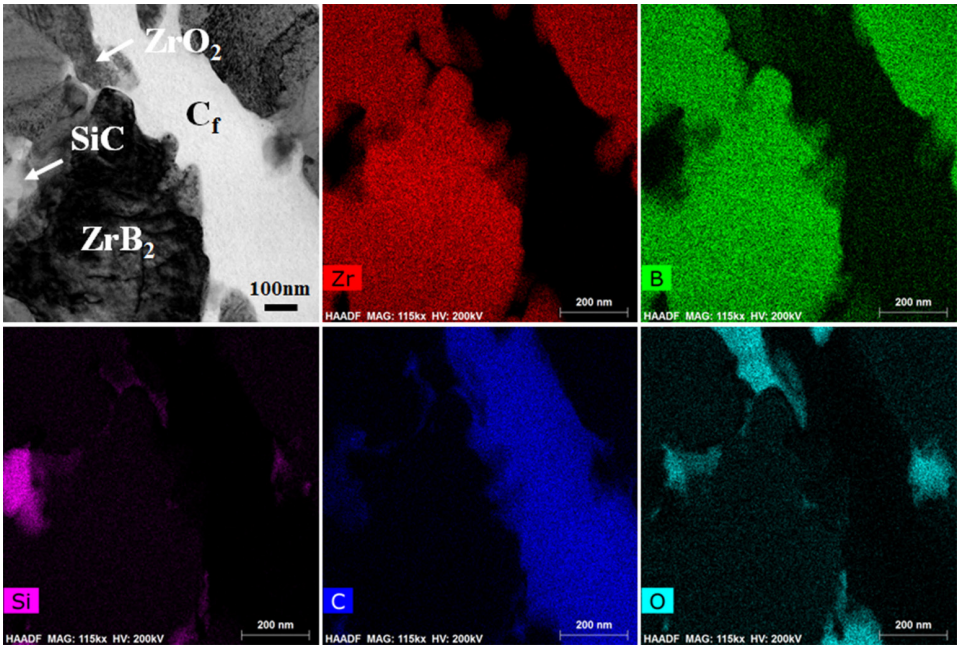

Fig. 4 Bright field image and element distribution on the observed area of ZSC30 performed by TEM showing phases present.

the starting ZrB_2 powders as shown by the X-ray diffraction pattern in Fig. 1. Typical ZrB_2/C_f, SiC/C_f, and ZrO_2/C_f interfaces of ZSC30 as well as the original structure of the raw carbon fiber are characterized by HR-TEM as shown in Fig. 5. The carbon fiber in ZSC30 has a typical non-ordered graphite structure of T800 carbon fiber [37] and the arrangement has no orderliness, which is similar to the original structure of the raw carbon fiber (Fig. 5(a)), implying a poor degree of graphitization in carbon fiber. The results indicate that the low sintering temperature of 1450 ℃ does not damage the intrinsic structure of the carbon fiber. It can be seen clear interfaces between carbon fibers and ceramic matrix, and no reaction products are detected in the interfaces, which implies that the reactions between carbon fibers and ceramic matrix are successfully inhibited.

3. 2 Mechanical properties

The relative densities and mechanical properties of ZrB_2–SiC–C_f composites are summarized in Table 2. The relative densities of ZrB_2–SiC–C_f composites decrease as the fiber content increases, which is consistent with the microstructures of the samples. The results indicate that the addition of fibers has a negative effect on the densification of ZrB_2-based ceramics, which might be attributed to the fiber bridging effect during hot pressing [38]. High relative densities of 98.2% and 97.1% are obtained for ZSC20 and ZSC30, respectively, much higher than those of ZSC40 and ZSC50 (85.7% and 80.4%, respectively), suggesting that an appropriate controlling of fiber content is essential to fabricate ZrB_2–SiC–C_f composites with high relative density. The relatively high density of ZSC20 is attributed to the nanosized ZrB_2 powders and the low carbon fiber content. On the one hand, the sinterability of the nanosized ZrB_2 powders is dramatically higher than that of their micron sized counterparts. On the other hand, fiber clumping generally occurs in ZrB_2–SiC–C_f composites when the carbon fiber content is more than 40 vol%, which would impede the densification of the composites during hot pressing process. From Fig. 2, it is clearly seen that the carbon fibers are uniformly distributed in the ZrB_2–SiC matrix without fiber clumping, suggesting that the addition of 20 vol% carbon fibers has minor effect on the densification of the ZrB_2–SiC matrix. Thereby, a relatively high density is obtained for the sample ZSC20 compared to the other published papers [39,40].

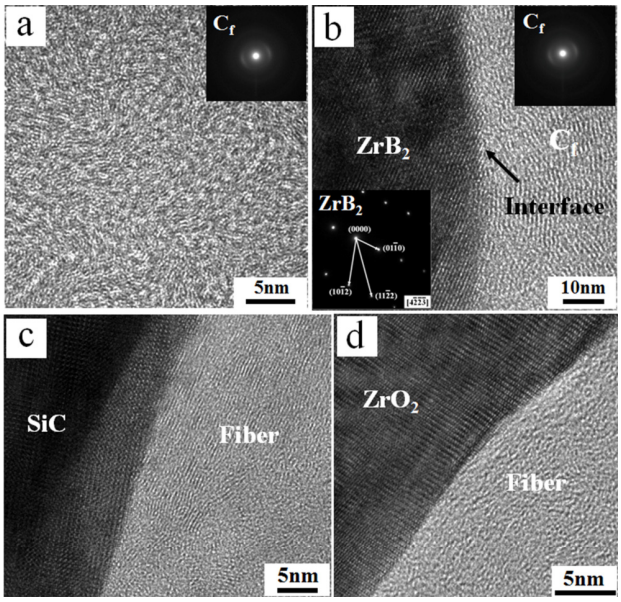

Fig. 5 HR-TEM images of (a) original structure of the raw carbon fiber and (b) ZrB_2/C_f, (c) SiC/C_f, and (d) ZrO_2/C_f interfaces of ZSC30, showing a typical non-ordered graphite structure of C_f and clear fiber/ceramic interfaces. The insets in (a) and (b) are the SAED patterns of C_f and ZrB_2.

The flexural strength of the ZrB_2–SiC–C_f composites decreases slightly from 375±18 MPa for ZSC20 to 325±12 MPa for ZSC30, while it decreases remarkably to 154±7 and 98±4 MPa for ZSC40 and ZSC50, respectively. The critical crack sizes of the ZrB_2–SiC–C_f composites as shown in Table 2 are calculated by the Griffith fracture criterion [41] based on fracture mechanism theory in terms of half crack length α_{cr}:

$$\alpha_{cr} \approx \frac{K_{IC}^2}{\sigma^2 \pi} \tag{1}$$

where α_{cr} is the critical crack size, σ is the critical stress which would cause the propagation of a crack-like flaw, and K_{IC} is the fracture toughness. With the increasing fiber content, the critical crack sizes

Table 2 Relative densities, mechanical properties, and calculated critical crack sizes of ZrB_2–SiC–C_f composites, showing high relative densities and mechanical properties for ZSC20 and ZSC30 compared with ZSC40 and ZSC50

Sample	Relative density (%)	Flexural strength (MPa)	Fracture toughness ($MPa \cdot m^{1/2}$)	K_{IC}/σ	Critical crack size (μm)
ZSC20	98.2	375±18	5.20±0.19	0.014	61.2
ZSC30	97.1	325±12	5.87±0.17	0.018	103.9
ZSC40	85.7	154±7	3.12±0.10	0.020	130.7
ZSC50	80.4	98±4	2.26±0.05	0.023	169.3

of the ZrB_2–SiC–C_f composites increase significantly from 61.2 (ZSC20) to 169.3 μm (ZSC50). According to the Griffith fracture criterion [41], the fracture of brittle ceramics should result from the propagation of inherent flaws with sizes beyond the critical crack size, leading to the catastrophic failures of ceramics. Therefore, the increase in the critical crack size of ZrB_2–SiC–C_f composite is valuable to improve the resistance to crack propagation in this composite.

Figure 6 displays the typical SEM images of crack propagation paths on the surfaces of ZSC30 under the fracture toughness and flexural strength testing. It is worth noting that the tested bars do not fracture into two parts after testing indicating that the composite has a great ability to avoid catastrophic breakage, which might be attributed to some toughening mechanisms, such as crack deflection, crack branching, fiber pullout, and fiber bridging as indicated by arrows in Fig. 6. It is believed that these mechanisms, especially crack deflection, can extend the crack path and absorb crack-propagating energy [42].

The effect of fiber content on the flexural stress–strain response of ZrB_2–SiC–C_f composites is displayed in Fig. 7. As indicated, ZSC20 exhibits a typical brittle fracture mode, while ZSC30, ZSC40, and ZSC50 show non-brittle fracture mode. The failure strain of the composites significantly increases with the increasing fiber content, and it achieves 0.32% for ZSC50, about 3 times higher than that of ZSC20 (0.10%). Additionally, the elastic modulus of the composites (evaluated as the slope of the flexural stress–strain curve before fracture in Fig. 7) decreases with the increasing fiber content, which is beneficial to improve the thermal shock resistance of the composites [43].

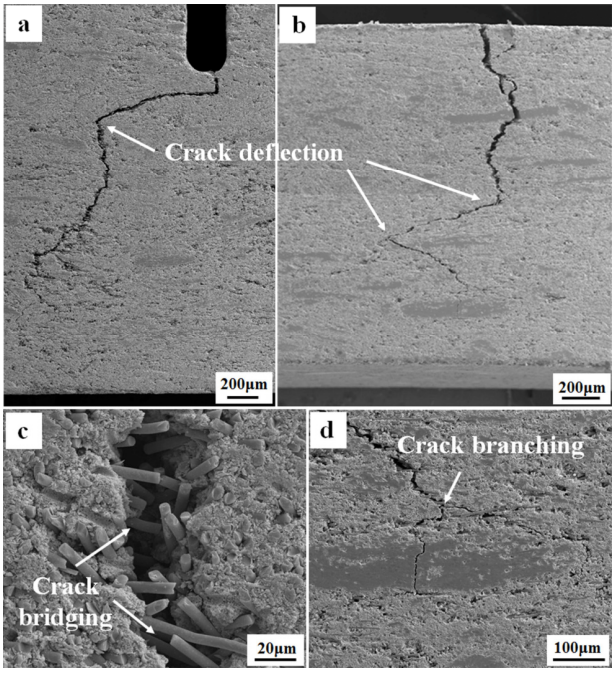

Fig. 6 Crack propagation on the polished surfaces of ZSC30 revealing (a, b) crack deflection, (c) crack bridging, and (d) crack branching mechanisms.

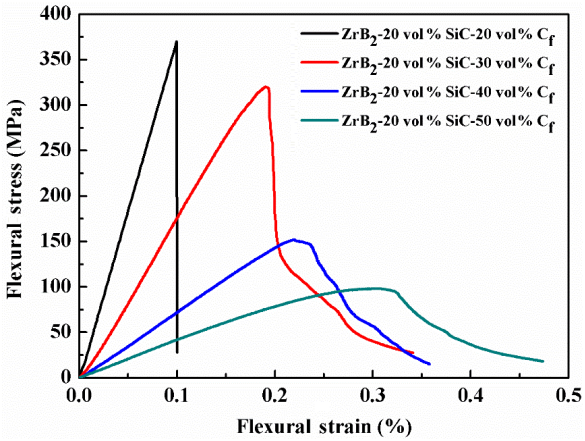

Fig. 7 Flexural stress–strain response of ZrB_2–SiC–C_f composites with different fiber contents, displaying the increased failure strain and the decreased elastic modulus with the increasing fiber content.

3.3 Thermal shock resistance

Considering that ZrB_2–SiC–C_f composites exhibit better mechanical properties when controlling the fiber content at 20–30 vol% as demonstrated above, ZSC20 and ZSC30 were selected to investigate their thermal shock resistance using water-quenching method. In a parallel test, the thermal shock behavior of ZrB_2–20 vol% SiC containing 15 vol% graphite (G) composite which was reported to have a good thermal shock resistance [44–46] was also investigated as a reference. Figure 8 shows the residual strengths of ZrB_2–SiC–G and ZrB_2–SiC–C_f composites after quenching at different temperature differences. As indicated, the residual strength of ZrB_2–SiC–G composite decreases slightly as the temperature difference increases from 0 to 300 ℃, while it decreases sharply to 37% of the initial strength at a temperature difference of 400 ℃, and the critical temperature difference of this composite is 345 ℃ which is higher than that of ZrB_2–SiC ceramics (ΔT_c = 290 ℃) [47] and lower than that of ZrB_2–SiC_f ceramics with Si_3N_4 addition (ΔT_c =400–500 ℃) [48]. In contrast, the residual strength value almost keeps stable as the temperature difference increases from 0 to 500 ℃ and

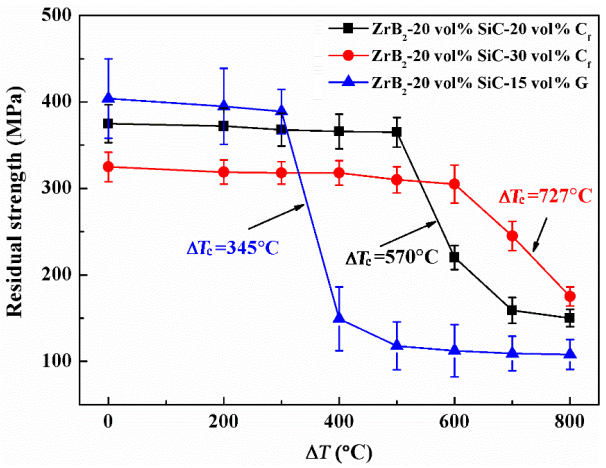

Fig. 8 Residual strength vs. thermal shock temperature difference for ZrB_2–20 vol% SiC–15 vol% G, ZSC20, and ZSC30, showing a high critical temperature difference (727 ℃) for ZSC30.

600 ℃ for ZSC20 and ZSC30, respectively, and then reduces gradually with further increased temperature difference. Despite having a lower initial strength, the ZrB_2–SiC–C_f composite water-quenched at a temperature difference of 400 ℃ or above has a much higher residual strength than that of the ZrB_2–SiC–G composite water-quenched at the same temperature difference.

A critical temperature difference of 570 ℃ is achieved for ZSC20, significantly higher than that of the ZrB_2–SiC–G composite (ΔT_c =345 ℃). Surprisingly, the critical temperature difference of ZSC30 is up to 727 ℃, much higher than the reported values of the ZrB_2-based UHTCs in previous literatures [47–50]. In order to further understand the excellent thermal shock resistance of ZrB_2–SiC–C_f composite, the thermal stress damage resistance parameter (R'''') is used to evaluate the thermal shock stress crack propagation of ceramics [51], represented by Eq. (2):

$$R'''' = \frac{E\gamma_f}{\sigma^2(1-\upsilon)} = \frac{K_{IC}^2}{\sigma^2(1-\upsilon)} \quad (2)$$

where σ is the tensile strength, E is the Young's modulus, γ_f is the fracture surface energy, and υ is the Poisson's ratio. R'''' indicates the resistance to catastrophic crack propagation of ceramics under a critical temperature difference. A higher K_{IC}/σ ratio rather than K_{IC} value represents a greater resistance to catastrophic crack propagation during rapid quenching which would result in a better thermal shock resistance of material. Therefore, the increased K_{IC}/σ ratio of ZrB_2–SiC–C_f composite with increasing fiber content (Table 2) should be responsible for the excellent thermal shock resistance of this composite. In addition, no micro-cracks are found on the surfaces of ZSC20 (not shown) and ZSC30 (shown in Fig. 9) after being water-quenched with different temperature differences, which also demonstrates that these composites have good resistance for crack initiation and crack propagation during rapid quenching.

3.4 Oxidation behavior

An appropriate controlling of the volume fraction of carbon fibers in the fabrication of ZrB_2–SiC–C_f composite is crucial to ensure a good oxidation resistance of the composite. In order to investigate the

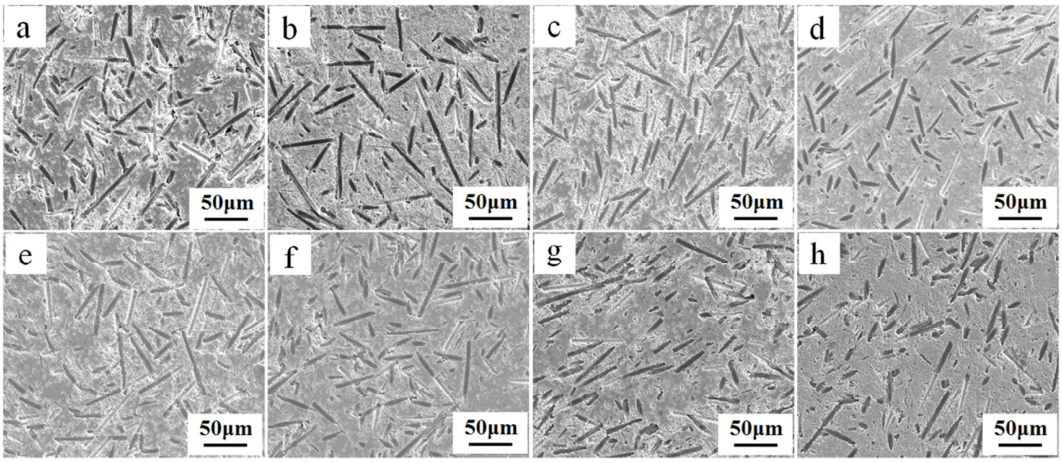

Fig. 9 SEM images of the sample ZSC30 after being water-quenched with different temperature differences: (a) 0 ℃, (b) 200 ℃, (c) 300 ℃, (d) 400 ℃, (e) 500 ℃, (f) 600 ℃, (g) 700 ℃, and (h) 800 ℃. No micro-cracks are found on these samples indicating a good resistance for crack initiation and crack propagation during rapid quenching.

oxidation resistance of ZrB_2–SiC–C_f composite, ZSC30, ZSC40, and ZSC50 were selected and oxidized at 1500 ℃ in static air for 1 h. Figure 10 shows the microstructures of the surfaces and cross-sections of the samples after oxidation. As indicated in Figs. 10(a)–10(c), a dense SiO_2 layer (detected by EDS) is generated on the surfaces of ZSC30 and ZSC40, while some pores are clearly observed on the surface of ZSC50. Figures 10(d) and 10(e) further show that dense SiO_2 layers with thicknesses of 5–10 μm isolate the inner ZrB_2–SiC–C_f composites from the outer environment when the fiber content is controlled at 40 vol% or below, which could protect the composites from further oxidation. However, excessive oxidation occurs in ZrB_2–SiC–C_f composite containing 50 vol% C_f because the protective SiO_2 layer falls off from a large area of the surface of the composite, leaving behind a porous ZrO_2 layer on the surface which could not protect the composite from further oxidation (Fig. 10(f)). Actually, the amount of the SiO_2 phase derived from the oxidation of SiC phase is sufficient to fill in the pores generated by the oxidation of carbon fibers existed on the surfaces of ZSC30 and ZSC40. However, a large body of pores on the surface of the composite could not be fully covered by the SiO_2 phase when 50 vol% carbon fibers are added. In the present study, ZrB_2–SiC ceramics containing ~40 vol% C_f exhibit excellent oxidation resistance, which provides great opportunities for the high temperature applications of these composites.

4 Conclusions

ZrB_2–SiC–C_f composites with 20–50 vol% carbon fibers uniformly distributed in ceramic matrix were successfully fabricated by hot pressing at 1450 ℃ using nanosized ZrB_2 powders (150 nm), in which the degradation of carbon fibers was effectively inhibited due to the low sintering temperature.

The relative density of the composite was above 95% when the fiber content was below 30 vol%, while it decreased with further increase of fiber content.

The flexural strength and fracture toughness of ZrB_2–SiC–C_f composite decreased with increasing fiber content, while the calculated critical crack size and the pullout length of carbon fiber both increased significantly.

The critical temperature difference of the composite containing 30 vol% C_f was up to 727 ℃, much higher than those of the reported ZrB_2-based UHTCs, and the composite displayed a good oxidation resistance when controlling fiber content at 40 vol% or below.

This work indicates that low temperature hot pressing of nanosized powders provides great potential in preparation of carbon fiber reinforced ultra-high temperature ceramics with excellent properties.

Acknowledgements

Financial support of this work was provided by the Innovative Research Group of National Natural Science

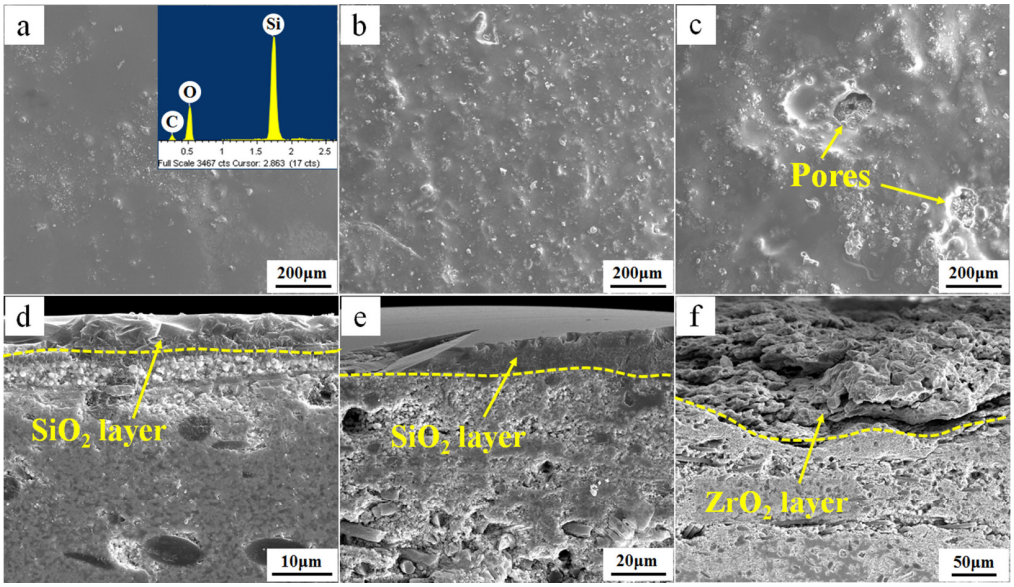

Fig. 10 SEM images of the surfaces and cross-sections of (a, d) ZSC30, (b, e) ZSC40, and (c, f) ZSC50 after oxidation at 1500 ℃ in static air for 1 h, showing a good oxidation resistance for ZSC30 and ZSC40.

Foundation of China (No. 11421091), the National Fund for Distinguished Young Scholars (No. 51525201), and the Fundamental Research Funds for the Central Universities (Grant No. HIT.BRETIII.201506).

References

[1] Guo S-Q. Densification of ZrB_2-based composites and their mechanical and physical properties: A review. *J Eur Ceram Soc* 2009, **29**: 995–1011.

[2] Lin J, Huang Y, Zhang H. Crack-healing and pre-oxidation behavior of ZrO_2 fiber toughened ZrB_2-based ceramics. *Int J Refract Met H* 2015, **48**: 5–10.

[3] Zou J, Zhang G-J, Shen Z-J, *et al*. Ultra-low temperature reactive spark plasma sintering of ZrB_2–*h*BN ceramics. *J Eur Ceram Soc* 2016, **36**: 3637–3645.

[4] Zamharir MJ, Asl MS, Vafa NP, *et al*. Significance of hot pressing parameters and reinforcement size on densification behavior of ZrB_2–25 vol% SiC UHTCs. *Ceram Int* 2015, **41**: 6439–6447.

[5] Zhang X, Liu R, Xiong X, *et al*. Mechanical properties and ablation behavior of ZrB_2–SiC ceramics fabricated by spark plasma sintering. *Int J Refract Met H* 2015, **48**: 120–125.

[6] Wang Z, Wang S, Zhang X, *et al*. Effect of graphite flake on microstructure as well as mechanical properties and thermal shock resistance of ZrB_2–SiC matrix ultrahigh temperature ceramics. *J Alloys Compd* 2009, **484**: 390–394.

[7] Monteverde F. Beneficial effects of an ultra-fine α-SiC incorporation on the sinterability and mechanical properties of ZrB_2. *Appl Phys A* 2006, **82**: 329–337.

[8] Wang Z, Wu Z, Shi G. Fabrication, mechanical properties and thermal shock resistance of a ZrB_2–graphite ceramic. *Int J Refract Met H* 2011, **29**: 351–355.

[9] Silvestroni L, Sciti D, Melandri C, *et al*. Toughened ZrB_2-based ceramics through SiC whisker or SiC chopped fiber additions. *J Eur Ceram Soc* 2010, **30**: 2155–2164.

[10] Lin J, Zhang X, Wang Z, *et al*. Microstructure and mechanical properties of ZrB_2–SiC–ZrO_{2f} ceramic. *Scripta Mater* 2011, **64**: 872–875.

[11] Yang F, Zhang X, Han J, *et al*. Mechanical properties of short carbon fiber reinforced ZrB_2–SiC ceramic matrix composites. *Mater Lett* 2008, **62**: 2925–2927.

[12] Zhu S, Fahrenholtz WG, Hilmas GE, *et al*. Pressureless sintering of carbon-coated zirconium diboride powders. *Mat Sci Eng A* 2007, **459**: 167–171.

[13] Zhou SB, Wang Z, Sun X, *et al*. Microstructure, mechanical properties and thermal shock resistance of zirconium diboride containing silicon carbide ceramic toughened by carbon black. *Mater Chem Phys* 2010, **122**: 470–473.

[14] Balak Z, Asl MS, Azizieh M, *et al*. Effect of different additives and open porosity on fracture toughness of ZrB_2–SiC-based composites prepared by SPS. *Ceram Int* 2017, **43**: 2209–2220.

[15] Asl MS, Golmohammadi F, Kakroudi MG, *et al*. Synergetic effects of SiC and C_{sf} in ZrB_2-based ceramic composites. Part I: Densification behavior. *Ceram Int* 2016, **42**: 4498–4506.

[16] Balak Z, Zakeri M, Rahimipour M, *et al*. Taguchi design and hardness optimization of ZrB_2-based composites reinforced with chopped carbon fiber and different additives and prepared by SPS. *J Alloys Compd* 2015, **639**: 617–625.

[17] Asl MS, Kakroudi MG, Farahbakhsh I, *et al*. Synergetic effects of SiC and C_{sf} in ZrB_2-based ceramic composites. Part II: Grain growth. *Ceram Int* 2016, **42**: 18612–18619.

[18] Yadhukulakrishnan GB, Rahman A, Karumuri S, *et al*. Spark plasma sintering of silicon carbide and multi-walled carbon nanotube reinforced zirconium diboride ceramic composite. *Mat Sci Eng A* 2012, **552**: 125–133.

[19] Asl MS, Farahbakhsh I, Nayebi B. Characteristics of multi-walled carbon nanotube toughened ZrB_2–SiC ceramic composite prepared by hot pressing. *Ceram Int* 2016, **42**: 1950–1958.

[20] Asl MS, Kakroudi MG, Kondolaji RA, *et al*. Influence of graphite nano-flakes on densification and mechanical properties of hot-pressed ZrB_2–SiC composite. *Ceram Int* 2015, **41**: 5843–5851.

[21] Yadhukulakrishnan GB, Karumuri S, Rahman A, *et al*. Spark plasma sintering of graphene reinforced zirconium diboride ultra-high temperature ceramic composites. *Ceram Int* 2013, **39**: 6637–6646.

[22] Asl MS, Kakroudi MG. Characterization of hot-pressed graphene reinforced ZrB_2–SiC composite. *Mat Sci Eng A* 2015, **625**: 385–392.

[23] Song G-M, Li Q, Wen G-W, *et al*. Mechanical properties of short carbon fiber-reinforced TiC composites produced by hot pressing. *Mat Sci Eng A* 2002, **326**: 240–248.

[24] Silvestroni L, Fabbriche DD, Melandri C, *et al*. Relationships between carbon fiber type and interfacial domain in ZrB_2-based ceramics. *J Eur Ceram Soc* 2016, **36**: 17–24.

[25] Yang F, Zhang X, Han J, *et al*. Processing and mechanical properties of short carbon fibers toughened zirconium diboride-based ceramics. *Mater Design* 2008, **29**: 1817–1820.

[26] Yang F, Zhang X, Han J, *et al*. Mechanical properties of short carbon fiber reinforced ZrB_2–SiC ceramic matrix composites. *Mater Lett* 2008, **62**: 2925–2927.

[27] Yang F, Zhang X, Han J, *et al*. Characterization of hot-pressed short carbon fiber reinforced ZrB_2–SiC ultra-high temperature ceramic composites. *J Alloys Compd* 2009, **472**: 395–399.

[28] Guo S, Naito K, Kagawa Y. Mechanical and physical behaviors of short pitch-based carbon fiber-reinforced HfB_2–SiC matrix composites. *Ceram Int* 2013, **39**: 1567–1574.

[29] Zamora V, Ortiz AL, Guiberteau F, *et al*. Crystal-size dependence of the spark-plasma-sintering kinetics of ZrB_2 ultra-high-temperature ceramics. *J Eur Ceram Soc* 2012, **32**: 271–276.

[30] Zamora V, Ortiz AL, Guiberteau F, *et al*. Spark-plasma sintering of ZrB_2 ultra-high-temperature ceramics at lower

temperature via nanoscale crystal refinement. *J Eur Ceram Soc* 2012, **32**: 2529–2536.
[31] Walker LS, Pinc WR, Corral EL. Powder processing effects on the rapid low-temperature densification of ZrB_2–SiC ultra-high temperature ceramic composites using spark plasma sintering. *J Am Ceram Soc* 2012, **95**: 194–203.
[32] Lee S-H, Yun J-Y, Oh HC, *et al*. Low temperature densification of ZrB_2 by the mechanical pre-treatment of particles. *J Ceram Soc Jpn* 2013, **121**: 480–486.
[33] Zimmermann JW, Hilmas GE, Fahrenholtz WG. Thermal shock resistance of ZrB_2 and ZrB_2–30% SiC. *Mater Chem Phys* 2008, **112**: 140–145.
[34] Silvestroni L, Sciti D, Melandri C, *et al*. Toughened ZrB_2-based ceramics through SiC whisker or SiC chopped fiber additions. *J Eur Ceram Soc* 2010, **30**: 2155–2164.
[35] He X, Guo Y, Zhou Y, *et al*. Microstructures of short-carbon-fiber-reinforced SiC composites prepared by hot-pressing. *Mater Charact* 2008, **59**: 1771–1775.
[36] Zheng G, Sano H, Suzuki K, *et al*. A TEM study of microstructure of carbon fiber/polycarbosilane-derived SiC composites. *Carbon* 1999, **37**: 2057–2062.
[37] Zhou X, You Y, Zhang C, *et al.* Effect of carbon fiber pre-heat-treatment on the microstructure and properties of C_f/SiC composites. *Mat Sci Eng A* 2006, **433**: 104–107.
[38] Sha JJ, Li J, Wang SH, *et al*. Toughening effect of short carbon fibers in the ZrB_2–$ZrSi_2$ ceramic composites. *Mater Design* 2015, **75**: 160–165.
[39] Sciti D, Zoli L, Silvestroni L, *et al*. Design, fabrication and high velocity oxy-fuel torch tests of a C_f–ZrB_2–fiber nozzle to evaluate its potential in rocket motors. *Mater Design* 2016, **109**: 709–717.
[40] Nasiri Z, Mashhadi M, Abdollahi A. Effect of short carbon fiber addition on pressureless densification and mechanical properties of ZrB_2–SiC–C_{sf} nanocomposite. *Int J Refract Met H* 2015, **51**: 216–223.
[41] Taylor D, Cornetti P, Pugno N, The fracture mechanics of finite crack extension. *Eng Fract Mech* 2005, **72**: 1021–1038.
[42] Fabert KT, Evans AG. Crack deflection processes—I. Theory. *Acta Metall* 1983, **31**: 565–576.
[43] Aldridge M, Yeomans JA. The thermal shock behaviour of ductile particle toughened alumina composites. *J Eur Ceram Soc* 1999, **19**: 1769–1775.
[44] Wang Z, Hong C, Zhang X, *et al*. Microstructure and thermal shock behavior of ZrB_2–SiC–graphite composite. *Mater Chem Phys* 2009, **113**: 338–341.
[45] Jin X, Zhang X, Han J, *et al*. Residual strength of a low-strength ceramic with a precrack induced by thermal shock. *J Am Ceram Soc* 2014, **97**: 691–694.
[46] Jin X, Zhang X, Han J, *et al*. Thermal shock behavior of porous ZrB_2–SiC ceramics. *Mat Sci Eng A* 2013, **588**: 175–180.
[47] Zhou P, Wang Z, Fan Y, *et al*. Thermal shock resistance of laminated ZrB_2–SiC ceramic evaluated by indentation technique. *J Am Ceram Soc* 2015, **98**: 2866–2872.
[48] Sciti D, Silvestroni L, Saccone G, *et al.* Effect of different sintering aids on thermo-mechanical properties and oxidation of SiC fibers–Reinforced ZrB_2 composites. *Mater Chem Phys* 2013, **137**: 834–842.
[49] Hou Y, Hu P, Zhang X, *et al*. Effects of graphite flake diameter on mechanical properties and thermal shock behavior of ZrB_2–nanoSiC–graphite ceramics. *Int J Refract Met H* 2013, **41**: 133–137.
[50] Li W, Zhang Y, Zhang X, *et al*. Thermal shock behavior of ZrB_2–SiC ultra-high temperature ceramics with addition of zirconia. *J Alloys Compd* 2009, **478**: 386–391.
[51] Hasselman DPH. Strength behavior of polycrystalline alumina subjected to thermal shock. *J Am Ceram Soc* 1970, **53**: 490–495.